

All in One: RGB, RGB-D, and RGB-T Salient Object Detection

Xingzhao Jia
Hefei University of Technology
Hefei, China
jxz625@126.com

Zhongqiu Zhao*
Hefei University of Technology
Hefei, China
z.zhao@hfut.edu.cn

Changlei Dongye
Shandong University of Science and Technology
Qingdao, China
dycl@sdust.edu.cn

Zhao Zhang
Hefei University of Technology
Hefei, China
cszzhang@gmail.com

Abstract

Salient object detection (SOD) aims to identify the most attractive objects within an image. Depending on the type of data being detected, SOD can be categorized into various forms, including RGB, RGB-D (Depth), RGB-T (Thermal) and light field SOD. Previous researches have focused on saliency detection with individual data type. If the RGB-D SOD model is forced to detect RGB-T data it will perform poorly. We propose an innovative model framework that provides a unified solution for the salient object detection task of three types of data (RGB, RGB-D, and RGB-T). The three types of data can be handled in one model (all in one) with the same weight parameters. In this framework, the three types of data are concatenated in an ordered manner within a single input batch, and features are extracted using a transformer network. Based on this framework, we propose an efficient lightweight SOD model, namely AiOSOD, which can detect any RGB, RGB-D, and RGB-T data with high speed (780FPS for RGB data, 485FPS for RGB-D or RGB-T data). Notably, with only 6.25M parameters, AiOSOD achieves excellent performance on RGB, RGB-D, and RGB-T datasets.

1. Introduction

Salient Object Detection (SOD) can locate the most salient objects in an image, and it is widely used as an important preprocessing method for many vision tasks such as image/video segmentation [11, 37], video compression [7], and visual tracking [10]. Depending on the data to be processed, SOD can be divided into 2D (RGB) SOD and 3D (RGB-D, RGB-T) SOD. 3D SOD addresses challenging scenarios by introducing depth maps or thermal maps paired with RGB maps.

Given the detection requirements for RGB, RGB-D, and RGB-T data, current models [2, 9, 19, 21, 43–45] can only handle a single type of data, and it cannot handle these three types of data simultaneously. Therefore, it is necessary to develop a model framework that can simultaneously meet the detection requirements for these three types of data. The model adopting this framework only needs to be trained once, and then it can use the same set of weight parameters to detect RGB, RGB-D, and RGB-T data.

In general, RGB SOD [15, 43, 45] requires only one network to extract RGB features, while RGB-D or RGB-T SOD [19, 21, 44] requires two networks to extract features from two modalities separately. The 3D SOD model differs from the 2D SOD model in that it includes an additional feature learning network and a multi-modal feature fusion module. To achieve the detection of three types of data in one model, this model needs to be optimized based on a 3D SOD framework to effectively handle RGB, RGB-D, and RGB-T data. When processing RGB data, the multi-modal feature fusion module has less impact on the RGB saliency prediction results because it processes learned RGB features, which is equivalent to fusing multiple RGB features. Therefore, it is only necessary to consider feature extraction methods that can be used for RGB, RGB-D, and RGB-T data to simplify the model structure while ensuring performance.

In the training process, we consider the depth map or thermal map as a special kind of RGB map and merge them into an input batch with the RGB maps in an orderly manner, and extract the features with one transformer network as the backbone network, as shown in Fig. 1. The network learns features from different modalities by sharing weights, and replaces the Batchnorm with the Layer-norm thus avoiding the interference of batch normalisation in learning features from different modalities. As shown

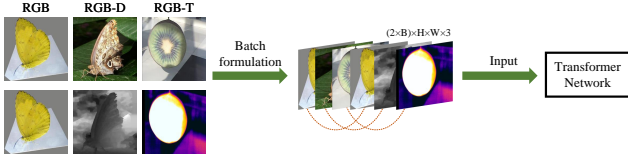


Figure 1. Diagram of proposed model framework. The framework extracts RGB, RGB-D, and RGB-T data simultaneously with a single transformer network with shared weights.

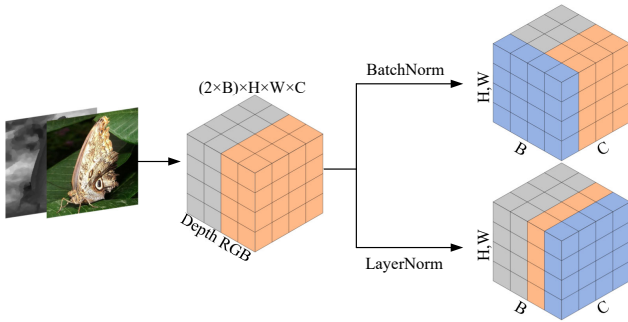


Figure 2. BatchNorm and LayerNorm.

in Fig. 2, a feature is obtained by concatenating RGB and Depth features in the Batch dimension. When BatchNorm is applied to this feature, the information from both modalities interferes with each other, whereas when LayerNorm is used, there is no interference. In summary, using a single transformer network with shared weights to extract multi-modal features can prevent negative interference between the modalities, ensuring performance, and simplifying the model structure, effectively saving parameters. Therefore, this feature extraction method is suitable for single-modal RGB information as well as dual-modal RGB-D and RGB-T information.

We build a lightweight SOD model based on the proposed model framework, which is called AiOSOD due to its ability to perform saliency detection for all three data types in one model. Due to the large training sets of the three data, AiOSOD is designed to be lightweight in order to validate the experimental results faster. AiOSOD employs a lightweight T2T-ViT-10 network [38] as the encoder and piggybacks on a lightweight decoder.

In conclusion, this paper has the following contributions:

- This work is the first time to consider all three (RGB, RGB-D, and RGB-T) saliency detection tasks all in one model. For the task of saliency detection of three different types of data, we introduces a novel model framework. This innovative model framework provides a unified solution for three types of data. It means that one weight file obtained through once training can be used universally for RGB, RGB-D, and RGB-T SOD. And the framework is successfully migrated in some 3D SOD models.

- Proposed framework employs a single-stream transformer network with shared weight parameters for extracting multi-modal features. This feature extraction method ensures comprehensive training for all three data types while preventing interference between multi-modal features. This not only provides a unified solution for the detection of all three data types but also ensures precision in detecting these data types. In comparison to models trained on only a single type of data, this framework achieves close performance and even make breakthroughs on some datasets. The effectiveness of this framework has been validated by our proposed model (AiOSOD).
- We propose a simple general model called AiOSOD to validate the proposed model framework. Thanks to the joint training of the three types of data and the feature extraction method, even though AiOSOD is a lightweight model, it achieves state-of-the-art performance in all three saliency detection tasks.

2. Related work

CNN-based SOD methods have achieved many impressive results. In recent years, transformer networks have evolved in the field of computer vision, demonstrating excellent performance. The transformer structure is commonly used to model global remote dependencies between word sequences in machine translation tasks [29]. The self-attention mechanism is the core idea of transformer, which establishes associations between different positions in a sequence by calculating the correlation between a query and a key. Transformer captures long-distance dependencies by stacking multiple layers of self-attention layers. Vision Transformer (ViT) [4] is the first application of the transformer structure to image classification tasks, being able to understand images from a holistic point of view. The ViT is suitable for a variety of vision tasks such as high-level classification and low-level dense prediction. Salient object detection belongs to the pixel-level dense prediction task. Therefore, more and more saliency detection models [13, 19, 21] have adopted the transformer structure to capture the global correlation information in images.

JL-DCF [9] first introduces siamese networks into RGB-D SOD, which employs a single convolutional network with shared parameters to extract common features of the two modalities. However, during training, the batch of JL-DCF can only be set to 1. If the batch size exceeds 1, its performance will decrease significantly. CSNet [41] employs a large kernel convolutional neural network as a siamese network to improve the performance. CCFENet [17] introduces a cross-modal interaction module on the basis of weight sharing to enhance the siamese network’s ability to learn features. However, neither of CSNet and CCFENet solve the problems of JL-DCF. In contrast, SiaTrans [13] addresses this issue. It finds that multimodal features inter-

fering with each other due to the effects of batch normalisation in multiple batches of training. SiaTrans adopts the transformer network as the siamese network, which conquers this drawback, makes full use of the computational power of the GPU and improves the training efficiency. Based on this property of the transformer, we can infer that the transformer network is suitable for the joint training of RGB, RGB-D, and RGB-T data.

3. Proposed model

In order to achieve saliency detection across three types of data, we propose a lightweight AiOSOD model (as illustrated in Fig. 3). The model is mainly composed of three components: an encoder, a token fusion module (TFM), and a decoder. The encoder employs the T2T-ViT-10 network with 5.31M parameters. The token fusion module facilitates high-level cross-modal information integration, containing 0.29M parameters. The decoder, structured with convolutional architecture, consists of three feature fusion modules (FFM) and a multi-level feature fusion module (MFFM), totally containing 0.64M parameters.

3.1. Encoder

Considering the performance and parameters of networks like ViT [4], T2T-ViT [38], PVTv2 [32], and Swin Transformer [20], we adopt the T2T-ViT-10 in the work [38] as the backbone network for our AiOSOD model. T2T-ViT [38] is an improvement for the lack of local modeling capability of ViT [4]. T2T-ViT incorporates the Tokens-to-Token (T2T) operation, which merges adjacent tokens into new tokens, effectively reducing token length and enabling local dependency modeling within images.

The token sequence $T_0 \in \mathbb{R}^{l \times c}$ derives from input image $I \in \mathbb{R}^{h \times w \times c}$ after undergoing transformations, and serves as the input of the backbone network. Through successive transformer operations and Tokens-to-Token (T2T) processes, multilevel tokens sequences, namely T_1, T_2 , and T_3 , are generated.

$$T_i = \text{Backbone}(T_0), \quad (1)$$

where $i = 1, 2, 3$. In order to reduce the parameters, T_i is subsequently dimensionally transformed to be 64. After that T_i needs to be split in the order of concatenating of input I to obtain T_{i1}, T_{i2} sequentially, as shown in Fig. 3.

$$T_{i1}, T_{i2} = \text{Split}(T_i). \quad (2)$$

T_{i1} and T_{i2} need to be reshaped into four-dimensional tensors to serve as inputs for the decoder consisting of a convolutional architecture. Additionally, T_{31} and T_{32} also serve as inputs of the tokens fusion module.

The tokens fusion module (TFM), as depicted in Fig. 3, is employed to integrate top-level tokens information, with

a parameter count of 0.288M. Generally, with equivalent parameters, the computational complexity of a transformer block significantly exceeds that of a convolutional block. Therefore, considering computation and performance comprehensively, AiOSOD only fuses the top-level tokens of the two modalities.

The ‘‘scaled dot-product attention’’ [4] in the multi-head attention can be written as:

$$\text{Attention}(Q, K, V) = \text{softmax}(QK^T / \sqrt{d_k})V, \quad (3)$$

where Q is Query, K is Key, V is Value, d_k is the length of the Key vector. AiOSOD may have three types of inputs, which are (RGB, RGB) pairs, (RGB, depth) pairs, and (RGB, thermal) pairs. When the input consists of RGB and depth modalities, according to Eq. (3), TFM facilitates cross-modal interaction through the following process:

$$\begin{aligned} \text{Attention}(Q_R, K_D, V_D) &= \text{softmax}(Q_R K_D^T / \sqrt{d_k})V_D, \\ \text{Attention}(Q_D, K_R, V_R) &= \text{softmax}(Q_D K_R^T / \sqrt{d_k})V_R. \end{aligned} \quad (4)$$

Similarly, RGB-T flows can be processed according to Eq. (4). When the input involves two RGB flows, the Key and Value of these two RGB flows are the same. TFM essentially reinforces self-attention for RGB tokens individually. Exactly because TFM can effectively handle different information flow pairs, which is highly suitable for AiOSOD, we adopt TFM to fuse the top-level tokens.

3.2. Decoder

The decoder of the AiOSOD model consists of three feature fusion modules (FFM) and one multi-level feature fusion module (MFFM). The schematic diagrams of FFM and MFFM are provided in Fig. 3. The parameters of FFM is 0.071M, while that of MFFM is of 0.141M.

The FFM within the decoder serves not only as component modules that aggregate features from high to low levels in the decoder network but also effectively fuse features. Each FFM module is composed of a CBAM attention [33] and two convolutional blocks. Through element-wise addition and multiplication, the FFM enhances salient features.

The multi-level feature fusion module (MFFM) is employed to fuse the three distinct-level features obtained from the FFMs, enhancing the accuracy of predictions. These features obtained from the FFMs, denoted as F_1, F_2 , and F_3 respectively, are upsampled to the size of (56×56) , maintaining the same dimensions as F_3 . Subsequently, the three features are fused using channel-wise attention and convolutional computations within the MFFM to achieve multi-level feature fusion.

3.3. Implementation details

Training dataset. AiOSOD is trained jointly using three different types of data. The training dataset consists of the

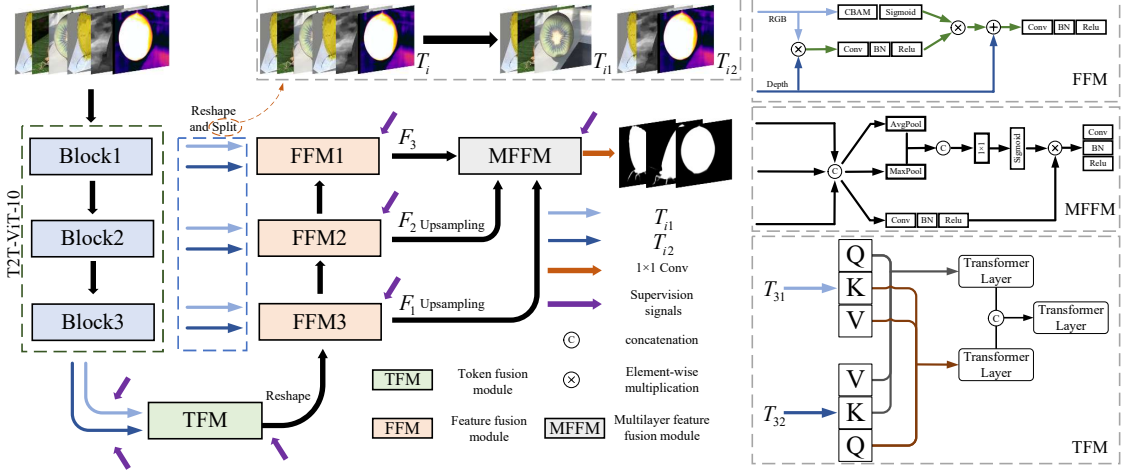


Figure 3. Framework of our proposed AiOSOD.

following subsets: the RGB dataset DUTS-TR [31] with 10,553 images, the RGB-T dataset VT5000 [28] with 2,500 image pairs, the RGB-D dataset NJUD [14] with 1,485 image pairs, NLPR [24] with 700 image pairs, and DUTLF-Depth [25] with 800 image pairs.

Loss function. We utilize the cross-entropy loss function:

$$\mathcal{L}(P, G) = - \sum_i [g_i \log(p_i) + (1 - g_i) \log(1 - p_i)], \quad (5)$$

where $P \in [0, 1]^{224 \times 224}$ and $G \in [0, 1]^{224 \times 224}$ represent the prediction map and ground truth (GT) map, respectively. $g_i \in G$, $p_i \in P$ represent individual pixel values.

Training settings. Our proposed model is implemented by PyTorch [23], and trained on an RTX2080Ti (11GB). We resize each image to 256×256 pixels and then randomly crop 224×224 image regions as the model input. We employ the Adam optimizer [16] with an initial learning rate of 0.0001 and a batch size of 16. The training process includes 300,000 steps. The learning rate is reduced by a factor of 10 at steps 100,000 and 200,000.

4. Benchmarking evaluation result

In this study, we conduct benchmark tests on RGB datasets, RGB-D datasets, and RGB-T datasets. We compare AiOSOD against a total of 16 state-of-the-art (SOTA) models on these datasets.

4.1. Evaluation metrics

MAE. The mean absolute error (MAE) [1] represents the average absolute pixel difference between the saliency prediction map (P) and the ground truth map (G), and it is

calculated using the following formula:

$$MAE = \frac{1}{W \times H} \sum_{x=1}^W \sum_{y=1}^H |P(x, y) - G(x, y)|, \quad (6)$$

where, W and H represent the width and height of the saliency map, respectively. A smaller error indicates a closer match between the prediction and the ground truth, thus indicating a more accurate prediction.

F-Measure. The F-measure [1] is a comprehensive performance metric calculated as the weighted harmonic mean of precision and recall. The formula is as follows:

$$F\text{-measure} = \frac{(1 + \beta^2) \times \text{Precision} \times \text{Recall}}{\beta^2 \times \text{Precision} + \text{Recall}}, \quad (7)$$

where β is set to 0.3. We use the maximum F-measure as the evaluation metric, where a higher value indicates better prediction performance.

S-Measure. The S-measure [5] is particularly focused on evaluating the structural information within saliency maps and is considered closer to the human visual system than the F-measure. The formula for S-measure is expressed as:

$$S = \gamma S_0 + (1 - \gamma) S_\gamma, \quad (8)$$

where S_0 and S_γ denote region-aware and object-aware structural similarities, respectively. The parameter γ is set to a default value of 0.5. Absolutely, a higher S-measure value indicates more accurate predictions in terms of capturing structural information within the saliency maps.

E-Measure. The E-measure [6] is employed to quantify both global and local saliency differences and can be expressed as:

$$E_m = \frac{1}{W \times H} \sum_{x=1}^W \sum_{y=1}^H \phi(x, y), \quad (9)$$

where $\phi(\cdot)$ represents the enhanced consistency matrix operation. A larger value of E_m indicates a more accurate prediction.

FPS, Parameters, and FLOPs. In Tabs. 1 and 2, we calculate the FPS, parameters, and FLOPs for these methods. The FPS calculation code is sourced from MobileSal [34] and is tested on the same RTX2080Ti (11G) platform. The code for calculating the parameters and FLOPs is obtained from the Python library 'thop'.

4.2. Comparison with SOTA RGB, RGB-D, and RGB-T SOD models

In Tab. 1, we compare our model (AiOSOD) with some SOTA models on RGB, RGB-D, and RGB-T datasets, respectively. RGB datasets include the testset of DUTS [31] (5019 images), DUT-OMORN [36] (5166 images), and ECSSD [35] (1000 images). RGB SOD models include ICON (PAMI22 [45]), ITSD (CVPR20 [43]), RCSB (WACV22 [15]), VST (ICCV21 [19]), CII (TIP21 [18]), and CTD-Net (ACM MM21 [42]). RGB-D datasets include the testsets of DUTLF-Depth [25] (400 pairs of images), NJUD [14] (500 pairs of images), NLPR [24] (300 pairs of images), and SIP [8] (929 pairs of images). RGB-D SOD models include C2DFNet (IEEE TM [39]), CAVER (TIP23 [22]), CCFENet (TCSVT22 [17]), JL-DCF (PAMI [9]), SwinNet (TCSVT21 [21]), and VST. RGB-T datasets include the testset of VT5000 [28] (2500 pairs of images), along with VT821 [30] (821 pairs of images), and VT1000 [27] (1000 pairs of images). RGB-T SOD models include CCFENet, TNet (IEEE TM22 [3]), LSNet (TIP23 [44]), CSRNet (TCSVT21 [12]), SwinNet, and VST. And in Tab. 2 our model is compared with three lightweight RGB-D models, LSNet, DFM-Net (ACM MM21 [40]), and MobileSal (PAMI21 [34]).

Tabs. 1a to 1c, present the comparative results on the RGB, RGB-D, and RGB-T datasets, respectively. Overall, benefiting from the proposed model framework, AiOSOD demonstrates a competitive advantage on RGB, RGB-D, and RGB-T datasets. It achieves excellent performance with low parameters, low computation requirements and high speed. In terms of FPS, parameters and Flops, AiOSOD achieves the best results in RGB and RGB-D saliency detection methods, and it's second-best in RGB-T saliency detection. Regarding performance, AiOSOD delivers moderate performance on the RGB dataset. However, surprisingly, AiOSOD, as a lightweight model, achieves second-best performance across multiple datasets in RGB-D and RGB-T. The data in Tab. 1 demonstrates that AiOSOD is able to efficiently process RGB, RGB-D, and RGB-T data, maintaining a balance between performance, size and speed.

Tab. 2 shows the results of the comparison between AiOSOD and the three lightweight RGB-D SOD models

Table 1. Quantitative comparison of our model with other SOTA RGB, RGB-D, and RGB-T SOD methods on benchmark datasets. The best and second best results are highlighted in red and blue.

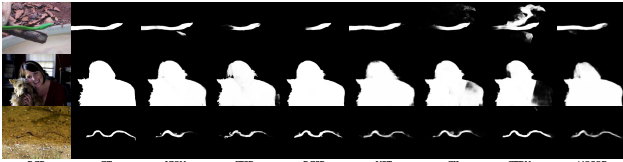
(a) RGB SOD methods							
Method	ICON	ITSD	RCSB	VST	CII	CTDNet	AiOSOD
Backbone	ResNet50	ResNet50	ResNet50	T2T-ViT-t14	ResNet18	ResNet18	T2T-ViT-10
Speed(FPS)	182	90	—	76	293	551	780
Params(M)	31.51	24.87	31.91	42.05	11.34	11.28	6.25
Flops(G)	19.53	14.87	265.12	21.64	14.89	5.72	2.04
DUT-OMORN							
$S_m \uparrow$	0.8442	0.8401	0.8350	0.8501	0.8388	0.8442	0.8447
$F_{\beta}^{max} \uparrow$	0.7985	0.7923	0.7727	0.8001	0.7817	0.7985	0.7890
$E_{\phi}^{max} \uparrow$	0.8842	0.8795	0.8659	0.8878	0.8757	0.8842	0.8823
$MAE \downarrow$	0.0569	0.0608	0.0492	0.0579	0.0538	0.0569	0.0549
DUTS-TE							
$S_m \uparrow$	0.8886	0.8849	0.8808	0.8961	0.8876	0.8886	0.8821
$F_{\beta}^{max} \uparrow$	0.8768	0.8680	0.8676	0.8779	0.8696	0.8768	0.8562
$E_{\phi}^{max} \uparrow$	0.9316	0.9294	0.9250	0.9393	0.9290	0.9316	0.9272
$MAE \downarrow$	0.0373	0.0410	0.0350	0.0374	0.0365	0.0373	0.0408
ECSSD							
$S_m \uparrow$	0.9290	0.9248	0.9217	0.9322	0.9261	0.9290	0.9280
$F_{\beta}^{max} \uparrow$	0.9433	0.9394	0.9355	0.9442	0.9395	0.9433	0.9387
$E_{\phi}^{max} \uparrow$	0.9603	0.9589	0.9545	0.9641	0.9562	0.9603	0.9623
$MAE \downarrow$	0.0318	0.0345	0.0335	0.0329	0.0334	0.0318	0.0339
(b) RGB-D SOD methods							
Method	C2DFNet	CAVER	CCFENet	JL-DCF	SwinNet	VST	AiOSOD
Backbone	ResNet50	ResNet50	ResNet50	ResNet50	Swin-B	T2T-ViT-t14	T2T-ViT-10
Speed(FPS)	283	144	46	17	21	58	485
Params(M)	45.31	53.21	27.33	118.76	189.57	79.21	6.25
Flops(G)	10.32	20.36	15.93	787.88	116.16	28.95	3.24
DUTLF-Depth							
$S_m \uparrow$	0.9326	0.9310	0.9328	0.8937	0.9469	0.9426	0.9455
$F_{\beta}^{max} \uparrow$	0.9440	0.9404	0.9445	0.8920	0.9579	0.9493	0.9526
$E_{\phi}^{max} \uparrow$	0.9638	0.9639	0.9636	0.9283	0.9752	0.9708	0.9746
$MAE \downarrow$	0.0252	0.0283	0.0263	0.0488	0.0226	0.0246	0.0239
NJUD							
$S_m \uparrow$	0.9079	0.9203	0.9165	0.9104	0.9255	0.9224	0.9248
$F_{\beta}^{max} \uparrow$	0.9086	0.9235	0.9210	0.9119	0.9283	0.9195	0.9233
$E_{\phi}^{max} \uparrow$	0.9423	0.9534	0.9543	0.9506	0.9573	0.9510	0.9567
$MAE \downarrow$	0.0389	0.0314	0.0323	0.0410	0.0314	0.0343	0.0330
NLPR							
$S_m \uparrow$	0.9279	0.9290	0.9268	0.9306	0.9296	0.9314	0.9273
$F_{\beta}^{max} \uparrow$	0.9166	0.9211	0.9184	0.9182	0.9170	0.9201	0.9115
$E_{\phi}^{max} \uparrow$	0.9605	0.9638	0.9624	0.9648	0.9624	0.9623	0.9582
$MAE \downarrow$	0.0217	0.0220	0.0208	0.0221	0.0225	0.0233	0.0250
SIP							
$S_m \uparrow$	0.8715	0.8934	0.8816	0.8852	0.9009	0.9036	0.9069
$F_{\beta}^{max} \uparrow$	0.8770	0.9064	0.8977	0.8935	0.9122	0.9150	0.9216
$E_{\phi}^{max} \uparrow$	0.9160	0.9344	0.9238	0.9305	0.9396	0.9439	0.9492
$MAE \downarrow$	0.0529	0.0424	0.0473	0.0490	0.0409	0.0396	0.0375
(c) RGB-T SOD methods							
Method	CCFENet	TNet	SwinNet	VST	LSNet	CSRNet	AiOSOD
Backbone	ResNet50	ResNet50	Swin-B	T2T-ViT-t14	MobileNetV2	ESPNetv2	T2T-ViT-10
Speed(FPS)	46	67	21	58	896	—	485
Params(M)	27.33	83.35	189.57	79.21	4.35	—	6.25
Flops(G)	15.93	51.13	116.16	28.95	1.15	4.20	3.24
VT800							
$S_m \uparrow$	0.8996	0.8989	0.8935	0.8832	0.8786	0.8847	0.9049
$F_{\beta}^{max} \uparrow$	0.8819	0.8884	0.8707	0.8541	0.8448	0.8579	0.8821
$E_{\phi}^{max} \uparrow$	0.9367	0.9382	0.9288	0.9172	0.9205	0.9226	0.9372
$MAE \downarrow$	0.0273	0.0302	0.0334	0.0412	0.0332	0.0376	0.0283
VT1000							
$S_m \uparrow$	0.9341	0.9286	0.9360	0.9329	0.9256	0.9183	0.9410
$F_{\beta}^{max} \uparrow$	0.9336	0.9296	0.9392	0.9314	0.9216	0.9083	0.9405
$E_{\phi}^{max} \uparrow$	0.9684	0.9662	0.9727	0.9705	0.9626	0.9525	0.9741
$MAE \downarrow$	0.0182	0.0212	0.0179	0.0211	0.0227	0.0242	0.0202
VT5000							
$S_m \uparrow$	0.8960	0.8952	0.9046	0.8870	0.8774	0.8677	0.8958
$F_{\beta}^{max} \uparrow$	0.8802	0.8809	0.8920	0.8610	0.8499	0.8372	0.8750
$E_{\phi}^{max} \uparrow$	0.9389	0.9374	0.9481	0.9286	0.9240	0.9138	0.9375
$MAE \downarrow$	0.0304	0.0328	0.0290	0.0383	0.0370	0.0416	0.0346

on NJUD and SIP datasets. Compared to the lightweight models DFM-Net, LSNet, and MobileSal, AiOSOD's parameters and FLOPs are slightly higher but it maintains the strongest performance. AiOSOD can process RGB-D images at 485 FPS, slower than DFM-Net and LSNet, and faster than MobileSal. It can be seen that AiOSOD is able to maintain high speed while maintaining a high accuracy.

As shown in Fig. 4, we demonstrate the generation of saliency maps in various challenging scenarios. Fig. 4a

Table 2. Comparison with lightweight RGB-D SOD models.

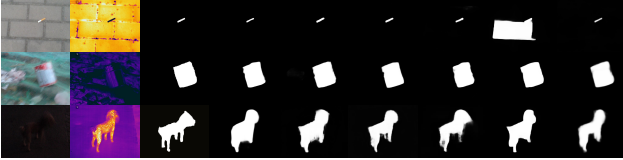
Method	DFM-Net	LSNet	MobileSal	AiOSOD
Backbone	MobileNetV2	MobileNetV2	MobileNetV2	T2T-ViT-10
Speed(FPS)	692	896	459	485
Params(M)	3.84	4.35	6.24	6.25
Flops(G)	2.68	1.15	1.51	3.24
NJUD				
$Sm \uparrow$	0.9072	0.9111	0.9097	0.9248
$F_{\beta}^{max} \uparrow$	0.9130	0.9144	0.9117	0.9233
$E_{\phi}^{max} \uparrow$	0.9525	0.9498	0.9502	0.9567
$MAE \downarrow$	0.0428	0.0386	0.0370	0.0330
SIP				
$Sm \uparrow$	0.8831	0.8861	0.8732	0.9069
$F_{\beta}^{max} \uparrow$	0.8873	0.8952	0.8795	0.9216
$E_{\phi}^{max} \uparrow$	0.9259	0.9306	0.9162	0.9492
$MAE \downarrow$	0.0507	0.0496	0.0528	0.0375



(a) RGB SOD methods



(b) RGB-D SOD methods



(c) RGB-T SOD methods

Figure 4. Qualitative comparison with SOTA RGB, RGB-D, and RGB-T SOD methods.

shows representative RGB images where AiOSOD consistently generates high-quality predictions, even in challenging conditions such as blurry boundaries, low contrast and small objects. Some representative RGB-D examples are shown in Fig. 4b. AiOSOD effectively utilizes depth information to enhance saliency detection, maintaining good performance even when the depth maps are blurry. Fig. 4c shows several representative RGB-T images.

5. Discussion

5.1. Function of proposed components

Tab. 3 presents the results of ablation experiments on these datasets concerning the proposed components. In these experiments, we start with a baseline model that adopts a clas-

Table 3. Quantitative evaluation results of ablation experiments for proposed components.

	Params(M)	DUTLF-Depth		VT821		ECSSD	
		$MAE \downarrow$	$F_{\beta}^{max} \uparrow$	$MAE \downarrow$	$F_{\beta}^{max} \uparrow$	$MAE \downarrow$	$F_{\beta}^{max} \uparrow$
Baseline	5.80	0.0308	0.9407	0.0366	0.8685	0.0356	0.9369
Base+TFM	6.10	0.0282	0.9434	0.0335	0.8788	0.0350	0.9378
Base+TFM+FFM	6.10	0.0264	0.9501	0.0321	0.8697	0.0370	0.9321
Base+TFM+FFM+MLF	6.25	0.0239	0.9526	0.0283	0.8821	0.0339	0.9387

sical U-shaped architecture, utilizing the TiT-ViT-10 network as the encoder and three dual convolution layers as the decoder. The baseline model also follows our proposed model framework and integrates cross-modal information through element-wise addition. From the experimental outcomes, it is evident that the baseline model performs well on the RGB, RGB-D, and RGB-T datasets, thanks to our proposed framework.

Subsequently, we add a tokens fusion module on the top level of the baseline model (Base+TFM model), which increases 0.3M parameters. Compared to the baseline model, Base+TFM model demonstrates performance improvements across all these datasets, affirming the effectiveness of the tokens fusion module.

Building upon Base+TFM model, we further introduce three feature fusion modules as model decoder (Base+TFM+FFM model). With very few additional parameters compared to the Base+TFM model, the Base+TFM+FFM model improves the detection of RGB-D and RGB-T data. However, due to the FFM’s primary focus on cross-modal feature fusion, its performance on the RGB dataset lags behind Base+TFM and baseline models.

In the final model (Base+TFM+FFM+MFFM model), we introduce a multi-level feature fusion module, namely AiOSOD. With this module, the performance of the model is successfully improved, thus improving all the metrics for the three types of datasets. Overall, these ablation experiment results confirm the effectiveness of our proposed model framework and individual components, showcasing their performance-enhancing effects across diverse datasets.

5.2. Function of proposed model framework

This subsection conducts experiments with JL-DCF [9] and VST [19] to explore the impact of extracting features with weight sharing in both convolutional and transformer networks. JL-DCF is the first RGB-D SOD model that extracts RGB and depth features through a convolutional network with shared weights, but its batch can only be set to 1. As shown in Fig. 2, the convolutional network uses BatchNorm to normalize the RGB and depth features in the batch dimension. The experimental results of JL-DCF are shown in Tab. 4. When batch size is 1, only one pair of RGB and depth features is normalized, which has little effect on the prediction results. However, when the batch size exceeds 1, more than one pair of RGB and depth features are normal-

Table 4. Impact of backbone network weight sharing on the prediction results of two RGB-D SOD models, JL-DCF and VST.

	Size (Mb)	Batch	NJUD		SIP		NLPR	
			MAE ↓	F_{β}^{max} ↑	MAE ↓	F_{β}^{max} ↑	MAE ↓	F_{β}^{max} ↑
JL-DCF	475	1	0.0454	0.8975	0.0491	0.8890	0.0216	0.9176
	475	6	0.0511	0.9038	0.0614	0.8604	0.0292	0.9030
VST	320	6	0.0351	0.9195	0.0403	0.9150	0.0236	0.9201
	238	6	0.0324	0.9275	0.0395	0.9149	0.0234	0.9232

ized, which affect each other and cause performance degradation. For the VST model, using a single transformer network with weight sharing to extract multi-modal features produces results comparable to the original model and is not limited by batch size. These experiments confirm that convolutional networks are not suited to providing a unified solution for three data types and achieving optimal performance. Therefore, using a transformer network as the feature extraction network in our proposed model framework is undoubtedly the best choice to meet the task requirements.

Tab. 5 presents the results of AiOSOD models with different backbone networks (T2T-ViT-10 [38], PVTv2-B0 [32], and Swin Tiny [20]), including trained jointly on the RGB, RGB-D, and RGB-T datasets, as well as models trained separately on each of these datasets. Among these models based on PVTv2-B0 and Swin Tiny architectures, the original model structure is retained, and an additional FFM module is introduced. Of course, the number of convolutional kernels in each layer has also been adjusted based on the backbone network. Experimental results on T2T-ViT-10, PVTv2-B0, and Swin Tiny consistently show that joint training using all three data types produces better results compared to training on a single data type. This outcome can be attributed to the effectiveness of the proposed model framework, which not only reduces interference between different data types but also significantly increases the effective training sample size, thereby enhancing predictive performance. The data in Tab. 5 confirms that the proposed model framework not only offers a unified solution for all three data types but also improves performance metrics across various testing datasets.

5.3. Applying proposed model framework to other models

We apply the proposed model framework to two transformer-based 3D SOD models, VST [19] and SwinNet [21]. In addition, a CNN-based LSNet [44] (MobileV2Net [26]) is used as a control for comparison. VST, SwinNet, and LSNet are 3D SOD models, and VST also provides a version for RGB detection. Therefore, Tab. 6 presents the results of VST, SwinNet, and LSNet on RGB-D and RGB-T datasets, as well as the results of VST on RGB datasets. In Tab. 6, the first row of each model represents its original model architecture, and the first row of data is sourced from Tab. 1.

Table 5. Comparison of training results for AiOSOD models using different backbone networks. JT means joint training on RGB, RGB-D, and RGB-T datasets.

(a) RGB Datasets						
Backbone	T2T-ViT-10		PVTv2-B0		Swin Tiny	
	Train dataset	RGB	JT	RGB	JT	RGB
DUTS-TE						
Sm ↑	0.8786	0.8821	0.8790	0.8797	0.8905	0.8931
F_{β}^{max} ↑	0.8521	0.8562	0.8519	0.8539	0.8659	0.8701
E_{ϕ}^{max} ↑	0.9234	0.9272	0.9239	0.9262	0.9329	0.9365
MAE ↓	0.0418	0.0408	0.0418	0.0412	0.0387	0.0381
DUT-OMRON						
Sm ↑	0.8365	0.8447	0.8383	0.8472	0.8445	0.8535
F_{β}^{max} ↑	0.7773	0.7890	0.7772	0.7922	0.7854	0.8018
E_{ϕ}^{max} ↑	0.8728	0.8823	0.8746	0.8875	0.8788	0.8928
MAE ↓	0.0599	0.0549	0.0566	0.0531	0.0548	0.0528
(b) RGB-D Datasets						
Backbone	T2T-ViT-10		PVTv2-B0		Swin Tiny	
	Train dataset	RGB-D	JT	RGB-D	JT	RGB-D
NJUD						
Sm ↑	0.9136	0.9248	0.9133	0.9247	0.9207	0.9309
F_{β}^{max} ↑	0.9093	0.9233	0.9092	0.9241	0.9209	0.9316
E_{ϕ}^{max} ↑	0.9474	0.9567	0.9459	0.9552	0.9549	0.9619
MAE ↓	0.0386	0.0330	0.0395	0.0343	0.0366	0.0308
SIP						
Sm ↑	0.8971	0.9069	0.8876	0.9001	0.8949	0.9112
F_{β}^{max} ↑	0.9082	0.9216	0.8965	0.9116	0.9043	0.9243
E_{ϕ}^{max} ↑	0.9403	0.9492	0.9349	0.9427	0.9403	0.9515
MAE ↓	0.0423	0.0375	0.0471	0.0414	0.0439	0.0370
(c) RGB-T Datasets						
Backbone	T2T-ViT-10		PVTv2-B0		Swin Tiny	
	Train dataset	RGB-T	JT	RGB-T	JT	RGB-T
VT1000						
Sm ↑	0.9263	0.9410	0.9297	0.9388	0.9309	0.9428
F_{β}^{max} ↑	0.9251	0.9405	0.9312	0.9406	0.9293	0.9447
E_{ϕ}^{max} ↑	0.9654	0.9741	0.9694	0.9745	0.9699	0.9775
MAE ↓	0.0240	0.0202	0.0240	0.0202	0.0225	0.0187
VT5000						
Sm ↑	0.8803	0.8958	0.8793	0.8940	0.8851	0.9034
F_{β}^{max} ↑	0.8467	0.8750	0.8508	0.8753	0.8586	0.8880
E_{ϕ}^{max} ↑	0.9238	0.9375	0.9251	0.9379	0.9338	0.9457
MAE ↓	0.0404	0.0346	0.0414	0.0364	0.0377	0.0325

For the VST and SwinNet, the results of both models trained jointly (Dual-s-JT and Single-s-JT) outperform the results of the model trained with a single dataset (Dual-s-ST) on these datasets. Moreover, most metrics of the Single-s-JT model are superior to those of the Dual-s-JT model. Since VST and SwinNet use the transformer network as the backbone, dual-stream VST and SwinNet with joint training (Dual-s-JT) still achieve relatively good results. One of the learning networks of the dual-stream VST or SwinNet extracts RGB images, while the input to the other learning network is a mixture of RGB, depth, and thermal images. Although Dual-s-JT-VST and Dual-s-JT-SwinNet perform well on all three types of datasets, RGB saliency detection requires only a single-stream network. Therefore the proposed model framework is more suitable for saliency detection of RGB, RGB-D, and RGB-

Table 6. Applying proposed model framework to other models results. ST means training on a single type of data. JT means joint training on RGB, RGB-D, and RGB-T datasets. Dual-s and Single-s indicate that the model employs a dual-stream backbone network or a single-stream backbone network.

(a) RGB Datasets									
Model	DUTS-TE				DUT-OMRON				
	$Sm \uparrow$	$F_{\beta}^{max} \uparrow$	$E_{\phi}^{max} \uparrow$	$MAE \downarrow$	$Sm \uparrow$	$F_{\beta}^{max} \uparrow$	$E_{\phi}^{max} \uparrow$	$MAE \downarrow$	
VST	Single-s-ST	0.8961	0.8779	0.9393	0.0374	0.8501	0.8001	0.8878	0.0579
	Dual-s-JT	0.8993	0.8819	0.9390	0.0357	0.8597	0.8152	0.8962	0.0535
	Single-s-JT	0.8974	0.8806	0.9390	0.0364	0.8597	0.8183	0.8973	0.0544
SwinNet	Dual-s-ST	—	—	—	—	—	—	—	—
	Dual-s-JT	0.9025	0.8873	0.9403	0.0316	0.8675	0.8245	0.9048	0.0438
	Single-s-JT	0.9051	0.8915	0.9437	0.0312	0.8683	0.8268	0.9068	0.0458
LSNet	Dual-s-ST	—	—	—	—	—	—	—	—
	Dual-s-JT	0.8570	0.8262	0.9072	0.0498	0.8286	0.7700	0.8706	0.0611
	Single-s-JT	0.8564	0.8282	0.9075	0.0510	0.8293	0.7765	0.8769	0.0632

(b) RGB-D Datasets									
Model	NJUD				SIP				
	$Sm \uparrow$	$F_{\beta}^{max} \uparrow$	$E_{\phi}^{max} \uparrow$	$MAE \downarrow$	$Sm \uparrow$	$F_{\beta}^{max} \uparrow$	$E_{\phi}^{max} \uparrow$	$MAE \downarrow$	
VST	Dual-s-ST	0.9224	0.9195	0.9510	0.0343	0.9036	0.9150	0.9439	0.0396
	Dual-s-JT	0.9274	0.9241	0.9540	0.0324	0.9147	0.9231	0.9516	0.0342
	Single-s-JT	0.9301	0.9310	0.9589	0.0314	0.9120	0.9222	0.9504	0.0354
SwinNet	Dual-s-ST	0.9255	0.9283	0.9573	0.0314	0.9009	0.9122	0.9396	0.0409
	Dual-s-JT	0.9230	0.9277	0.9537	0.0338	0.9046	0.9158	0.9440	0.0385
	Single-s-JT	0.9274	0.9305	0.9578	0.0316	0.9156	0.9318	0.9537	0.0332
LSNet	Dual-s-ST	0.9111	0.9144	0.9498	0.0386	0.8861	0.8952	0.9306	0.0496
	Dual-s-JT	0.8786	0.8670	0.9171	0.0536	0.8730	0.8761	0.9251	0.0560
	Single-s-JT	0.8907	0.8847	0.9278	0.0512	0.8864	0.8886	0.9286	0.0521

(c) RGB-T Datasets									
Model	VT1000				VT5000				
	$Sm \uparrow$	$F_{\beta}^{max} \uparrow$	$E_{\phi}^{max} \uparrow$	$MAE \downarrow$	$Sm \uparrow$	$F_{\beta}^{max} \uparrow$	$E_{\phi}^{max} \uparrow$	$MAE \downarrow$	
VST	Dual-s-ST	0.9329	0.9314	0.9705	0.0211	0.8870	0.8610	0.9286	0.0383
	Dual-s-JT	0.9418	0.9443	0.9745	0.0192	0.9048	0.8891	0.9441	0.0317
	Single-s-JT	0.9418	0.9446	0.9751	0.0183	0.9048	0.8905	0.9461	0.0314
SwinNet	Dual-s-ST	0.9360	0.9392	0.9727	0.0179	0.9046	0.8920	0.9481	0.0290
	Dual-s-JT	0.9365	0.9380	0.9727	0.0190	0.9119	0.9032	0.9550	0.0261
	Single-s-JT	0.9449	0.9475	0.9785	0.0167	0.9191	0.9113	0.9590	0.0239
LSNet	Dual-s-ST	0.9256	0.9216	0.9626	0.0227	0.8774	0.8499	0.9240	0.0370
	Dual-s-JT	0.9264	0.9222	0.9613	0.0229	0.8843	0.8614	0.9288	0.0364
	Single-s-JT	0.9286	0.9266	0.9644	0.0224	0.8884	0.8708	0.9338	0.0367

T data. It's worth noting that the single-stream VST model shows an approximate 18% increase in training speed compared to the dual-stream VST model, and the model size decreases from 320MB to 238MB. Similarly, the single-stream SwinNet model exhibits about a 15% increase in training speed compared to the dual-stream SwinNet model, with the model size decreasing from 786MB to 441MB. The proposed model framework has successfully migrated on the VST and SwinNet, providing a unified solution for RGB, RGB-D, and RGB-T SOD, resulting in improved model performance and reducing parameters. Combining the experimental results of VST and SwinNet, the proposed model framework can be applied to other 3D SOD models, thus providing a unified solution for all three types of data and reducing model size.

Compared to the original LSNet (Dual-s-ST), LSNet (Single-s-JT) using a single-stream network with joint training exhibits performance decrease on the RGB-D dataset and an improvement on the RGB-T dataset. In Tab. 6, the LSNet trained jointly (Dual-s-JT and Single-s-JT) outperforms the original LSNet (Dual-s-ST) in the RGB-T dataset. We infer that this result is likely due to the similarity between thermal and RGB images, as both are three-channel images with rich color information. Due to the large proportion of RGB data in the joint training dataset,

Table 7. LSNet and MobileV2Net-based AiOSOD detection results on RGB-T dataset. JT means joint training on RGB, RGB-D, and RGB-T datasets. Dual-s and Single-s indicate that the model employs a dual-stream backbone network or a single-stream backbone network.

Model	Train Dataset	LSNet			AiOSOD		
		Dual-s RGB-T	Single-s RGB-T	Single-s JT	Dual-s RGB-T	Single-s RGB-T	Single-s JT
VT821	$Sm \uparrow$	0.8786	0.8783	0.9023	0.8408	0.8424	0.8984
	$F_{\beta}^{max} \uparrow$	0.8448	0.8524	0.8872	0.7822	0.7813	0.8759
	$E_{\phi}^{max} \uparrow$	0.9205	0.9226	0.9431	0.8786	0.8749	0.9392
	$MAE \downarrow$	0.0332	0.0376	0.0290	0.0641	0.0570	0.0315
VT1000	$Sm \uparrow$	0.9256	0.9210	0.9286	0.9133	0.9167	0.9332
	$F_{\beta}^{max} \uparrow$	0.9216	0.9186	0.9266	0.9070	0.9094	0.9329
	$E_{\phi}^{max} \uparrow$	0.9626	0.9618	0.9644	0.9535	0.9552	0.9704
	$MAE \downarrow$	0.0227	0.0262	0.0224	0.0289	0.0288	0.0234
VT5000	$Sm \uparrow$	0.8774	0.8784	0.8884	0.8496	0.8496	0.8883
	$F_{\beta}^{max} \uparrow$	0.8499	0.8553	0.8708	0.8035	0.8043	0.8647
	$E_{\phi}^{max} \uparrow$	0.9240	0.9313	0.9338	0.8955	0.8957	0.9337
	$MAE \downarrow$	0.0370	0.0387	0.0367	0.0511	0.0513	0.0380

the jointly trained model may perform better for RGB-T data because of this similarity. To confirm this inference, we conduct experiments by replacing the backbone network of AiOSOD with MobileV2Net [26]. This model, adapts for MobileV2Net, removing the TFM and MFFM modules, adding an additional FFM module. In Tab. 7, LSNet and AiOSOD both achieve optimal results by using a single-stream learning network and undergoing joint training. Moreover, when the training set contains only RGB-T data, Single-s-AiOSOD outperforms Dual-s-AiOSOD, and Single-s-LSNet performs close to Dual-s-LSNet. These experimental result confirms our inference. Additionally, it can be observed that when (RGB, thermal) pairs are concatenated in the batch dimension, batch normalization has a minor impact on the prediction results, unlike the case with RGB-D.

6. Conclusions

In this paper, we are the first to consider a unified solution to realize RGB, RGB-D and RGB-T SOD, requiring only one model and same weights to perform SOD on all three modalities. To achieve the unified solution, we propose a model framework and develop a lightweight model for validation (AiOSOD). The lightweight AiOSOD model demonstrates excellent performance on RGB, RGB-D, and RGB-T datasets, effectively balancing performance and speed. Our proposed model framework takes three types of data as the training set, concatenating them in the batch dimension and extracting features through a transformer network. With this framework, the model can learn from all three types of data and avoid performance degradation due to interference between multimodal features. Importantly, the proposed model framework can be applied to other 3D SOD models, reducing model size and providing a unified solution for RGB, RGB-D, and RGB-T SOD. In the future, we

will continue to explore more efficient unified solutions for SOD.

References

- [1] Ali Borji, Ming-Ming Cheng, Huaizu Jiang, and Jia Li. Salient object detection: A benchmark. *IEEE Transactions on Image Processing*, 24(12): 5706–5722, 2015. 4
- [2] Xiaolong Cheng, Xuan Zheng, Jialun Pei, He Tang, Zehua Lyu, and Chuanbo Chen. Depth-induced gap-reducing network for rgb-d salient object detection: An interaction, guidance and refinement approach. *IEEE Transactions on Multimedia*, pages 1–1, 2022. 1
- [3] Runmin Cong, Kepu Zhang, Chen Zhang, Feng Zheng, Yao Zhao, Qingming Huang, and Sam Kwong. Does thermal really always matter for rgb-t salient object detection? *IEEE Transactions on Multimedia*, pages 1–12, 2022. 5
- [4] Alexey Dosovitskiy, Lucas Beyer, Alexander Kolesnikov, Dirk Weissenborn, Xiaohua Zhai, Thomas Unterthiner, Mostafa Dehghani, Matthias Minderer, Georg Heigold, Sylvain Gelly, et al. An image is worth 16x16 words: Transformers for image recognition at scale. *arXiv preprint arXiv:2010.11929*, 2020. 2, 3
- [5] Deng-Ping Fan, Ming-Ming Cheng, Yun Liu, Tao Li, and Ali Borji. Structure-measure: A new way to evaluate foreground maps. In *Proceedings of the IEEE International Conference on Computer Vision (ICCV)*, 2017. 4
- [6] Deng-Ping Fan, Cheng Gong, Yang Cao, Bo Ren, Ming-Ming Cheng, and Ali Borji. Enhanced-alignment measure for binary foreground map evaluation. In *Proceedings of the Twenty-Seventh International Joint Conference on Artificial Intelligence, IJCAI-18*, pages 698–704. International Joint Conferences on Artificial Intelligence Organization, 2018. 4
- [7] Deng-Ping Fan, Wenguan Wang, Ming-Ming Cheng, and Jianbing Shen. Shifting more attention to video salient object detection. In *Proceedings of the IEEE/CVF Conference on Computer Vision and Pattern Recognition (CVPR)*, 2019. 1
- [8] Deng-Ping Fan, Zheng Lin, Zhao Zhang, Menglong Zhu, and Ming-Ming Cheng. Rethinking rgb-d salient object detection: Models, data sets, and large-scale benchmarks. *IEEE Transactions on Neural Networks and Learning Systems*, 32(5):2075–2089, 2021. 5
- [9] Keren Fu, Deng-Ping Fan, Ge-Peng Ji, Qijun Zhao, Jianbing Shen, and Ce Zhu. Siamese network for rgb-d salient object detection and beyond. *IEEE Transactions on Pattern Analysis and Machine Intelligence*, 44(9):5541–5559, 2022. 1, 2, 5, 6
- [10] Yuan Gao, Miaoqing Shi, Dacheng Tao, and Chao Xu. Database saliency for fast image retrieval. *IEEE Transactions on Multimedia*, 17(3):359–369, 2015. 1
- [11] Chenlei Guo and Liming Zhang. A novel multiresolution spatiotemporal saliency detection model and its applications in image and video compression. *IEEE Transactions on Image Processing*, 19(1):185–198, 2010. 1
- [12] Fushuo Huo, Xuegui Zhu, Lei Zhang, Qifeng Liu, and Yu Shu. Efficient context-guided stacked refinement network for rgb-t salient object detection. *IEEE Transactions on Circuits and Systems for Video Technology*, 32(5):3111–3124, 2022. 5
- [13] XingZhao Jia, ChangLei DongYe, and YanJun Peng. Siatrans: Siamese transformer network for rgb-d salient object detection with depth image classification. *Image and Vision Computing*, 127:104549, 2022. 2
- [14] Ran Ju, Ling Ge, Wenjing Geng, Tongwei Ren, and Gangshan Wu. Depth saliency based on anisotropic center-surround difference. In *2014 IEEE International Conference on Image Processing (ICIP)*, pages 1115–1119, 2014. 4, 5
- [15] Yun Yi Ke and Takahiro Tsubono. Recursive contour-saliency blending network for accurate salient object detection. In *Proceedings of the IEEE/CVF Winter Conference on Applications of Computer Vision (WACV)*, pages 2940–2950, 2022. 1, 5
- [16] Diederik P Kingma and Jimmy Ba. Adam: A method for stochastic optimization. *arXiv preprint arXiv:1412.6980*, 2014. 4
- [17] Guibiao Liao, Wei Gao, Ge Li, Junle Wang, and Sam Kwong. Cross-collaborative fusion-encoder network for robust rgb-thermal salient object detection. *IEEE Transactions on Circuits and Systems for Video Technology*, 32(11):7646–7661, 2022. 2, 5
- [18] Jiang-Jiang Liu, Zhi-Ang Liu, Pai Peng, and Ming-Ming Cheng. Rethinking the u-shape structure for salient object detection. *IEEE Transactions on Image Processing*, 30:9030–9042, 2021. 5
- [19] Nian Liu, Ni Zhang, Kaiyuan Wan, Ling Shao, and Junwei Han. Visual saliency transformer. In *Proceedings of the IEEE/CVF International Conference on Computer Vision (ICCV)*, pages 4722–4732, 2021. 1, 2, 5, 6, 7
- [20] Ze Liu, Yutong Lin, Yue Cao, Han Hu, Yixuan Wei, Zheng Zhang, Stephen Lin, and Baining Guo. Swin transformer: Hierarchical vision transformer using shifted windows. In *Proceedings of the IEEE/CVF International Conference on Computer Vision (ICCV)*, pages 10012–10022, 2021. 3, 7
- [21] Zhengyi Liu, Yacheng Tan, Qian He, and Yun Xiao. Swinnet: Swin transformer drives edge-aware rgb-d

- and rgb-t salient object detection. *IEEE Transactions on Circuits and Systems for Video Technology*, 32(7): 4486–4497, 2022. 1, 2, 5, 7
- [22] Youwei Pang, Xiaoqi Zhao, Lihe Zhang, and Huchuan Lu. Cover: Cross-modal view-mixed transformer for bi-modal salient object detection. *IEEE Transactions on Image Processing*, 32:892–904, 2023. 5
- [23] Adam Paszke, Sam Gross, Francisco Massa, Adam Lerer, James Bradbury, Gregory Chanan, Trevor Killeen, Zeming Lin, Natalia Gimelshein, Luca Antiga, et al. Pytorch: An imperative style, high-performance deep learning library. *Advances in neural information processing systems*, 32, 2019. 4
- [24] Houwen Peng, Bing Li, Weihua Xiong, Weiming Hu, and Rongrong Ji. Rgb-d salient object detection: A benchmark and algorithms. In *Computer Vision – ECCV 2014*, pages 92–109, Cham, 2014. Springer International Publishing. 4, 5
- [25] Yongri Piao, Wei Ji, Jingjing Li, Miao Zhang, and Huchuan Lu. Depth-induced multi-scale recurrent attention network for saliency detection. In *Proceedings of the IEEE/CVF International Conference on Computer Vision (ICCV)*, 2019. 4, 5
- [26] Mark Sandler, Andrew Howard, Menglong Zhu, Andrey Zhmoginov, and Liang-Chieh Chen. Mobilenetv2: Inverted residuals and linear bottlenecks. In *Proceedings of the IEEE Conference on Computer Vision and Pattern Recognition (CVPR)*, 2018. 7, 8
- [27] Zhengzheng Tu, Tian Xia, Chenglong Li, Xiaoxiao Wang, Yan Ma, and Jin Tang. Rgb-t image saliency detection via collaborative graph learning. *IEEE Transactions on Multimedia*, 22(1):160–173, 2020. 5
- [28] Zhengzheng Tu, Yan Ma, Zhun Li, Chenglong Li, Jieming Xu, and Yongtao Liu. Rgbt salient object detection: A large-scale dataset and benchmark. *IEEE Transactions on Multimedia*, pages 1–1, 2022. 4, 5
- [29] Ashish Vaswani, Noam Shazeer, Niki Parmar, Jakob Uszkoreit, Llion Jones, Aidan N Gomez, Łukasz Kaiser, and Illia Polosukhin. Attention is all you need. *Advances in neural information processing systems*, 30, 2017. 2
- [30] Guizhao Wang, Chenglong Li, Yunpeng Ma, Aihua Zheng, Jin Tang, and Bin Luo. Rgb-t saliency detection benchmark: Dataset, baselines, analysis and a novel approach. In *Image and Graphics Technologies and Applications*, pages 359–369, Singapore, 2018. Springer Singapore. 5
- [31] Lijun Wang, Huchuan Lu, Yifan Wang, Mengyang Feng, Dong Wang, Baocai Yin, and Xiang Ruan. Learning to detect salient objects with image-level supervision. In *Proceedings of the IEEE Conference on Computer Vision and Pattern Recognition (CVPR)*, 2017. 4, 5
- [32] Wenhai Wang, Enze Xie, Xiang Li, Deng-Ping Fan, Kaitao Song, Ding Liang, Tong Lu, Ping Luo, and Ling Shao. Pvt v2: Improved baselines with pyramid vision transformer. *Computational Visual Media*, 8(3):415–424, 2022. 3, 7
- [33] Sanghyun Woo, Jongchan Park, Joon-Young Lee, and In So Kweon. Cbam: Convolutional block attention module. In *Proceedings of the European conference on computer vision (ECCV)*, pages 3–19, 2018. 3
- [34] Yu-Huan Wu, Yun Liu, Jun Xu, Jia-Wang Bian, Yu-Chao Gu, and Ming-Ming Cheng. Mobilesal: Extremely efficient rgb-d salient object detection. *IEEE Transactions on Pattern Analysis and Machine Intelligence*, 44(12):10261–10269, 2022. 5
- [35] Qiong Yan, Li Xu, Jianping Shi, and Jiaya Jia. Hierarchical saliency detection. In *Proceedings of the IEEE Conference on Computer Vision and Pattern Recognition (CVPR)*, 2013. 5
- [36] Chuan Yang, Lihe Zhang, Huchuan Lu, Xiang Ruan, and Ming-Hsuan Yang. Saliency detection via graph-based manifold ranking. In *Proceedings of the IEEE Conference on Computer Vision and Pattern Recognition (CVPR)*, 2013. 5
- [37] Linwei Ye, Zhi Liu, Lina Li, Liquan Shen, Cong Bai, and Yang Wang. Saliency object segmentation via effective integration of saliency and objectness. *IEEE Transactions on Multimedia*, 19(8):1742–1756, 2017. 1
- [38] Li Yuan, Yunpeng Chen, Tao Wang, Weihao Yu, Yujun Shi, Zi-Hang Jiang, Francis E.H. Tay, Jiashi Feng, and Shuicheng Yan. Tokens-to-token vit: Training vision transformers from scratch on imagenet. In *Proceedings of the IEEE/CVF International Conference on Computer Vision (ICCV)*, pages 558–567, 2021. 2, 3, 7
- [39] Miao Zhang, Shunyu Yao, Beiqi Hu, Yongri Piao, and Wei Ji. C²dfnet: Criss-cross dynamic filter network for rgb-d salient object detection. *IEEE Transactions on Multimedia*, pages 1–13, 2022. 5
- [40] Wenbo Zhang, Ge-Peng Ji, Zhuo Wang, Keren Fu, and Qijun Zhao. Depth quality-inspired feature manipulation for efficient rgb-d salient object detection. In *Proceedings of the 29th ACM International Conference on Multimedia*, page 731–740, New York, NY, USA, 2021. Association for Computing Machinery. 5
- [41] Yunhua Zhang, Hangxu Wang, Gang Yang, Jianhao Zhang, Congjin Gong, and Yutao Wang. Csnet: a convnext-based siamese network for rgb-d salient object detection. *The Visual Computer*, pages 1–19, 2023. 2
- [42] Zhirui Zhao, Changqun Xia, Chenxi Xie, and Jia Li. Complementary trilateral decoder for fast and accurate salient object detection. In *Proceedings of the 29th*

ACM International Conference on Multimedia, page 4967–4975, New York, NY, USA, 2021. Association for Computing Machinery. 5

- [43] Huajun Zhou, Xiaohua Xie, Jian-Huang Lai, Zixuan Chen, and Lingxiao Yang. Interactive two-stream decoder for accurate and fast saliency detection. In *Proceedings of the IEEE/CVF Conference on Computer Vision and Pattern Recognition (CVPR)*, 2020. 1, 5
- [44] Wujie Zhou, Yun Zhu, Jingsheng Lei, Rongwang Yang, and Lu Yu. Lsnet: Lightweight spatial boosting network for detecting salient objects in rgb-thermal images. *IEEE Transactions on Image Processing*, 32: 1329–1340, 2023. 1, 5, 7
- [45] Mingchen Zhuge, Deng-Ping Fan, Nian Liu, Dingwen Zhang, Dong Xu, and Ling Shao. Salient object detection via integrity learning. *IEEE Transactions on Pattern Analysis and Machine Intelligence*, 45(3):3738–3752, 2023. 1, 5